UNIVERSITY OF CALIFORNIA

Santa Barbara

Population of Tau Embedded in Parallel β-Sheets Depends on Heparin Stoichiometry

A Thesis submitted in partial satisfaction of the

requirements for the degree Master of Science

in Chemical Engineering

by

Zachary Ray Oberholtzer

Committee in charge:

Professor Songi Han, Chair

Professor M. Scott Shell

Professor Michelle A. O'Malley

December 2015

The thesis of Zachary Ray Oberholtzer is approved.

_____

M. Scott Shell

_____

Michelle A. O'Malley

_____

Songi Han, Committee Chair

ACKNOWLEDGEMENTS

I would like to thank my advisor, Professor Songi Han, for supporting and encouraging me throughout this endeavor. I would also like to thank my friends and family for making this life worth living.

ABSTRACT

Population of Tau Embedded in Parallel β-Sheets Depends on Heparin Stoichiometry

by

Zachary Ray Oberholtzer

The aggregation of the human tau protein is heavily implicated in the progression of Alzhiemer's Disease. In this study we examined the aggregation kinetics of a truncated segment of the longest tau isoform, Tau 187, and induced aggregation with the polyanion hepain. We applied cw-EPR in order to quantitatively measure the population of tau embedded in parallel β-sheet structure and compared these measurements to traditional kinetic measurement techniques, Tht fluorescence and turbidity. Cw-EPR revealed rapid formation of parallel β-sheet structure early in the aggregation process well before fibrils are thought to appear. We observe a large population of spins first exhibits reduced mobility upon mixing with heparin, which is later followed by an increase in β-sheet structure consistent with proposed models of nucleation followed by structural rearrangement. Additionally, comparing cw-EPR with Tht fluorescence demonstrates Tht binding is non-linear with respect to parallel β-sheet structure and the precise binding structure of Tht remains unclear.

The transfer of tau pathology from infected to healthy cells has been well established by the literature, however, little is known about the relationship between seed structure and seeding efficacy. Here we investigated the importance of β-sheet content as detected by cw-EPR on seeding efficacy, but were unable to establish a relationship due to the overriding

effect of heparin. Previously our group has observed a conformational shift around the PHF6* hexapeptide from compact to extended state and we examined the stoichiometric effect of heparin on this extension to determine the potency of heparin for inducing changes in the tau system. Finally, dependence of tau aggregation kinetics on heparin stoichiometry was investigated. We discovered the extent of observable distance change depended on heparin stoichiometry, however, even dilute quantities of heparin are able to induce significant extension around the PHF6* hexapeptide. The amount of total fibril formation was also found to depend on the heparin stoichiometry with lower heparin concentrations generating less total fibril content. Our findings suggests even minute quantities of heparin exerts great influence on the tau system and future work will require ways of working around or limiting heparin's influence in order to directly probe the underlying fundamentals of tau aggregation.

TABLE OF CONTENTS

LIST OF FIGURES

I. Introduction

Alzheimer's disease (AD) is the sixth leading cause of death in the United States, fifth for the 65 or older age group, and places a heavy burden on society both economically and emotionally for those with affected family members.[1] The aggregation of human tau, an intrinsically disordered protein (IDP), is strongly correlated with the progression of AD, in which tau fibrils are a hallmark of the disease pathology. Current therapeutic approaches for AD show little effectiveness for improving patient quality of life or arresting disease progression, thus improving our understanding of tau aggregation should aid in the development of effective treatments.[2, 3] Until recently the majority of AD research focused on amyloid-β, another aggregating protein heavily implicated in AD progression, the aggregation of which is generally thought to precede tau aggregation.[4, 5] Although tau has been placed downstream of amyloid-β aggregation evidence suggests tau is critically involved in mediating disease toxicity.[6, 7] Additionally, accumulation of tau aggregates correlates strongly with worsening patient condition, whereas accumulation of amyloid-β aggregates shows no such correlation.[8] Meanwhile, even the basic mechanism of tau aggregation is not known or agreed upon in the literature. This justifies the importance of studying the structural and dynamic properties of early intermediates of tau aggregation.

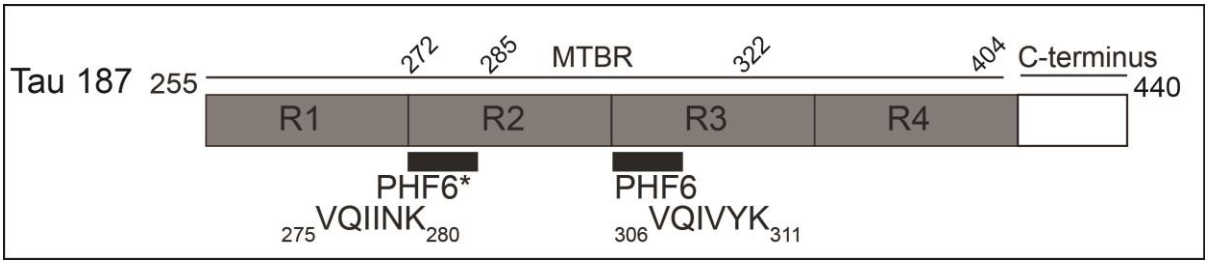

Figure 1: Schematic of the Tau 187 segment used in this study. The Tau187 segment is that of the longest tau isoform hTau40 with the n-terminus truncated, spanning the full microtubule binding region (MTBR). The two hexapeptide motifs and their location in the tau sequence are shown.

In this study, we focus on the aggregation of peptide and protein fragments of the human tau protein. Tau consists of six isoforms all of which are incorporated into fibrils during AD progression. The primary function of tau is binding and stabilizing microtubules, which provides structural integrity to the cell. Each tau isoform contains three or four repeat microtubule binding domains which are located in the C-terminus.[9] The aggregation of tau into fibrils is dependent on two hexapeptide motifs, sequence VQIINK (PHF6*) and VQIVYK (PHF6), which form the core of the β-sheet structure and are located in the microtubule binding region of the protein, Figure 1.[10, 11] The presence of one of the hexapeptides—certain tau isoforms only contain the PHF6 sequence—while critical are generally insufficient to promote aggregation at experimentally relevant time scales and the forces driving the normally soluble tau monomer to aggregate are unclear, especially *in vivo*.[12] In solution tau is intrinsically disordered with no overt secondary or tertiary structure, while it displays overall low hydrophobic character. The full length tau isoforms exhibit a small net charge; however, there are regions of the chain with high charge density, mainly in the repeat binding domain.[13] It is speculated that charge neutralization in the repeat binding domain allows for tau assembly; although, it should be noted that charge neutralization by adjusting pH is insufficient to induce aggregation at experimentally relevant time scales.[9, 13] In order to study tau at experimentally useful time scales generally truncated segments of the

full length isoforms are studied usually containing the microtubule binding regions with at least one of PHF6 or PHF6*. The addition of aggregation inducing cofactors, commonly polyanions, is usually required in addition to truncation in order for aggregation to proceed. The most common polyanion used in tau aggregation studies is heparin, which aggregates tau into fibrils morphologically similar to those found in AD.[10, 14, 15] This has led to the wide-spread usage of heparin in the literature for investigating tau aggregation. We will also use heparin as an initiator of tau aggregation in order to study early aggregation intermediates and kinetics of tau peptide and protein fragments.

The overarching goal of this study is to probe the nature of the aggregate seed and the driving force of tau aggregation. Insight into the interactions between naive tau, early aggregates and heparin will provide important clues into potential therapeutic approaches to prevent or slow down aggregation. Tau aggregation typically follows a sigmoidal kinetic profile with a distinct lag phase preceding a rapid growth phase which eventually tapers culminating with the appearance of mature fibrils, Figure 2.[16] Considerable study of aggregation kinetics has been carried out but in the absence of sufficiently direct probing tools the kinetics data of fibril formation gives important, but incomplete insight. Thioflavin T (Tht) is a fluorescent dye sensitive to amyloid structure and has been used to monitor tau aggregation kinetics.[17, 18] Despite its utility Tht cannot provide quantitative or clear assessment of β-sheet structure due to unresolved questions about its binding stoichiometry and mechanisms. Rather, Tht offers an empirical metric for assessing the content of certain β-sheet species, though the size threshold required for Tht fluorescence activity is unclear.

The unclear relationship between Tht fluorescence and other kinetic measurements—such as turbidity—with molecular level structural details necessitates the use of other tools

for monitoring aggregation. In this study we turn to continuous wave Electron Paramagnetic Resonance (cw-EPR) which through appropriate application can provide quantitative population measurements of tau molecules embedded in parallel β-sheet structure and additionally can be used to probe the local environment around the attached spin label.[19, 20] The application of cw-EPR allows for monitoring of specific structural features during the aggregation process including the difficult to detect early intermediates and provides population measurements of the total number of spins experiencing any one environment. Additionally, comparing cw-EPR measurements with Tht fluorescence will provide a more thorough understanding of the precise structural details Tht detects.

A key concept in tau aggregation is understanding the interaction between tau aggregates and tau monomer. The progression of AD is marked by the systematic and predictable spread of tau pathology along interconnected neural pathways.[21, 22] Multiple studies have shown in cell and mouse models that transfer of tau pathology from infected to healthy cells, whereby pre-formed aggregate "seeds" enter healthy cells and recruit endogenous tau into fibril aggregates, is possible by normal cellular processes.[22-28] . While this type of seeded aggregation mechanism does not explain the first cause of tau aggregation it provides a plausible mechanism for the propagation of tau and AD pathology. Considerable study of seeded aggregation has been focused *in vivo*, attempting

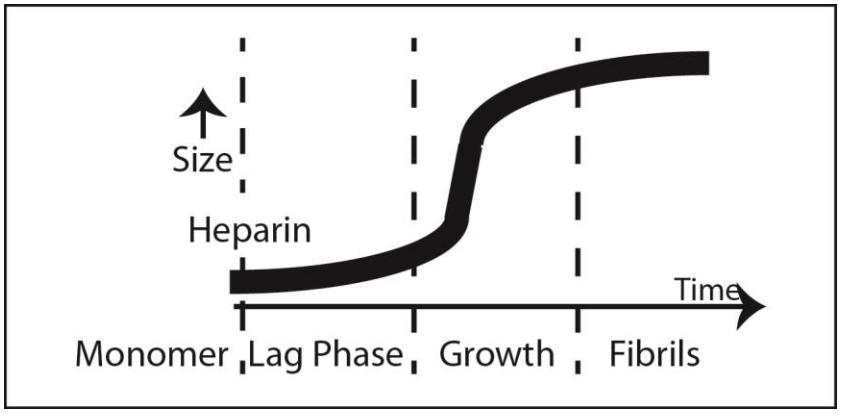

Figure 2: Schematic of typical sigmoidal kinetics of Tau aggregation induced with the polyanion heparin. Initially, little activity is detected followed by rapid increase in signal intensity which eventually reaches a maximum.

to identify tau oligomers/species which are capable of penetrating cell membranes and recruiting endogenous tau into fibril aggregates and elucidating cellular mechanisms of internalization and externalization.[23, 28] Seeded aggregation was demonstrated *in vitro* capable of reducing or eliminating the characteristic lag phase and as well as increasing the rate of aggregation.[16, 29, 30] However, these *in vitro* studies primarily have used late stage fibrils, often sonicated before exposing to naive tau, as the seed material and characterization of the seeds used in these studies has been lacking. While there has been some effort *in vivo* to identify the effect of different oligomer species on recruitment of endogenous tau, it is difficult to isolate the fundamental efficacy of oligomers and distinct conformations in inducing aggregation irrespective of the confounding effects of cellular process.[23, 28] We would like to approach this question from an *in vitro* perspective and investigate whether certain structural attributes, as measured by cw-EPR, change the interaction between aggregates and naïve tau.

In this work we investigated several characteristics of the tau aggregation process. We applied continuous wave Electron Paramagnetic Resonance (cw-EPR) to quantify and track the amount of tau population embedded in β-sheet content during aggregation and compared to more traditional Tht fluorescence measurements. Margetti and Langen first showed the utility of cw-EPR for analyzing tau fibrils by identifying a signature line shape for parallel β-sheet structure, which with proper analysis can be used to determine side-chain mobility and quantify % population involved in inter-molecular β-sheet contacts.[19] Additionally, we investigated the relationship between population of tau embedded in β-sheet structure, as measured by cw-EPR, and efficacy in recruiting naïve tau to form fibrils. Essentially we questioned whether the maturity of tau aggregates impacts the ability of seeds

to not only template aggregation but to additionally catalyze recruitment of tau monomer into fibrils. Finally, we investigate the stoichiometric role of heparin in inducing conformational rearrangement. Previously, our group has identified a conformational shift around the PHF6* hexapeptide from a compact hairpin like structure to an extended conformation upon incubation with heparin. We believe this conformational shift is a key step in the aggregation pathway. Double Electron Electron Resonance (DEER) spectroscopy was employed in order to examine conformational rearrangements around the PHF6* hexapeptide when mixed with different stoichiometric amounts of heparin. In this study we apply a combination of traditional techniques and the unique spectroscopy tools available to our lab in order to examine the early aggregation process and interrogate the effect of pre-formed aggregate seeds on naïve tau with the goal of improving understanding of tau aggregation.

II. Technical Background

2.1 Thioflavin T Fluorescence

Thioflavin T (Tht) has found considerable usage as a fluorescent dye for identification of amyloid structure with a relatively high degree of specificity. The predominant hypothesis of Tht binding posits Tht binds within channels created by the amino acid side chains involved in β-sheet formation, a prevalent structural component of amyloid. These channels run parallel to the long fibril axis of the β-sheet structure. The binding of Tht restricts the rotation of Tht's benzylamine and benzathiole rings. The rotation of these two rings quenches the excited states of Tht thus by restricting rotation the excited states are preserved and a many fold increase in fluorescence is observed.[18] The Tht fluorescence assay provides only a qualitative assessment of the total amount of fibril content.[17]

2.2 cw-EPR Line Shape Analysis

Continuous wave Electron Paramagnetic Resonance (cw-EPR) of proteins singly labeled with nitroxide radicals can be used to monitor changes in the protein backbone dynamics and the formation of inter-protein contacts. In this study we use the nitroxide (1-oxyl-2,2,5,5,-tetramethylpyrroline-3-methyl) methanethiosulfonate (MTSL) and its diamagnetic analog (EPR inactive) (1-Acetoxy-2,2,5,5,-tetramethyl-d-3-pyrroline-3-methyl) methanethiosulfonate, (dMTSL). The spin labels are attached to tau via a disulfide bond to cysteines selectively located within the amino acid sequence using site directed mutagenesis. Through line shape analysis of the EPR spectra individual side-chain mobility and quantitative determination of tau population embedded in parallel β-sheet content can be investigated. Singly labeled tau fibrils previously examined by cw-EPR have been shown to have spin-exchange broadening, a situation where the electron orbitals of the spin labels are close enough (<8Å) to overlap and a characteristic single line component contribution to the typical three line nitroxide EPR spectrum is observed, Figure 3A. The appearance of the spin-exchange interaction indicates the tau molecules are stacking in a parallel fashion.[19, 31] Validation of this conclusion is completed by spin dilution, mixing paramagnetic (MTSL)

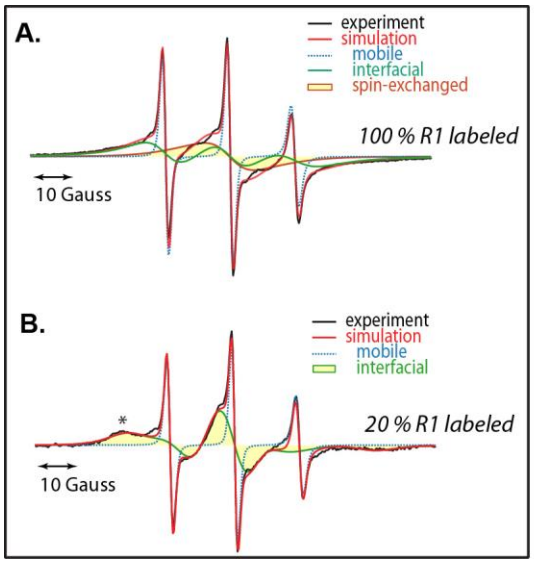

Figure 3: A) EPR nitroxide spectra of 100% MTSL labeled tau upon aggregation. Requires a three component fit including a spin-exchange component in addition to mobile and interfacial components. B) EPR nitroxide spectra of 20:80 ratio MTSL:dMTSL spin labeled tau upon aggregation. Only requires two component fit with mobile and interfacial components.

labeled tau with diamagnetic (dMTSL) tau in a 20:80 ratio which eliminates contributions from spin-exchange and reduces the effect of dipolar broadening, Figure 3B. As displayed in Figure 3 the 100% MTSL labeled tau requires a three component fit including a single line spin-exchange component which is indicative of parallel β-sheet, whereas the 20:80 spin diluted EPR spectrum only requires a two component fit and does not include a spin-exchange component. For reference monomeric MTSL labeled tau yields a sharp three line nitroxide spectrum which can be fit by a purely mobile component. The interfacial component represents spins which suffer reduced mobility but are not experiencing spin-exchange. Through simulation of the collected EPR spectrums the % population of tau involved in parallel β-sheet structure can be determined. The simulations conducted in this study were carried out using the Multicomponent software developed by Dr. Christian Altenbach (University of California, Los Angeles, CA).

2.3 DEER Spectroscopy

Double electron-electron resonance (DEER) can be used to measure distances between a pair of paramagnetic spin labels in the range of 1.7-10nm.[32, 33] Measuring distances using pulsed EPR techniques offer enhanced sensitivity compared to scattering

techniques and can measure longer distances than Nuclear Magnetic Resonance (NMR) which is typically limited to distances within 1nm.[34, 35] Fluorescence resonance energy transfer (FRET) is a popular biological technique for distance measurements and offers greater sensitivity compared to DEER, however, the labels used in FRET measurements are bulkier than the spin labels available for DEER and thus have a greater risk of perturbing the system being studied. FRET requires the use of two different chromophores, whereas DEER can measure distances between either the same type spin label or two different labels and labeling protocols can be much more difficult for FRET.[35] There are a few drawbacks of DEER which should be noted namely the need to conduct experiments at cryogenic temperatures, which forces the use of glass-forming agents such as glycerol or sucrose, and the use of deuterated buffers, which are necessary to extend the spin-spin diffusion time T_2 allowing greater sensitivity and longer distances to be measured.[36] Carrying out measurements at cryogenic temperatures is not necessarily a major disadvantage as it allows us to take a snap-shot of the transient aggregation process.

The pulse sequence used in this study is a four pulse DEER sequence, Figure 4A, which has the benefit of eliminating artifacts due to dead time. In practice DEER consists of measuring the amplitude of a refocused echo while sweeping the time placement, t, of the pump pulse, Figure 4A. The pulses at frequency ω_A are the observed channel and induce a refocused echo in the spin population affected by the ω_A frequency. The pump pulse at the ω_B frequency inverts a different spin population which modulates the refocused echo intensity at the dipolar frequency.

The dipolar frequency ν_{dd} is defined in eqn 1, where g_1, g_2 are the g values of the two spins, μ_B is the bohr magneton, μ_0 is the vacuum permeability, θ is the angle between the

spin-spin vector and the external field and r is the distance separating spins. In cases where there is no orientational selectivity, as should be the case for nitroxide spin labels attached to protein, θ is taken to be 90^0. The dipolar frequency can be determined from the fast Fourier transform of the background corrected trace, Figure 4B, where the dipolar frequency $2\nu_{dd}(r, 90°)$ is extracted from the pake pattern, Figure 4C, and related to the distance by eqn 2 with the constant values approximated for nitroxide spin labels.

$$\nu_{dd}(\theta, r) = \frac{\mu_0 g_1 g_2 \mu_B}{2h}(3\cos^2\theta + 1)\frac{1}{r^3} \quad 1$$

$$\nu_{dd}(\theta, r) = \sqrt[3]{\frac{52.16}{\nu_{dd}(r, 90°)}} \quad 2$$

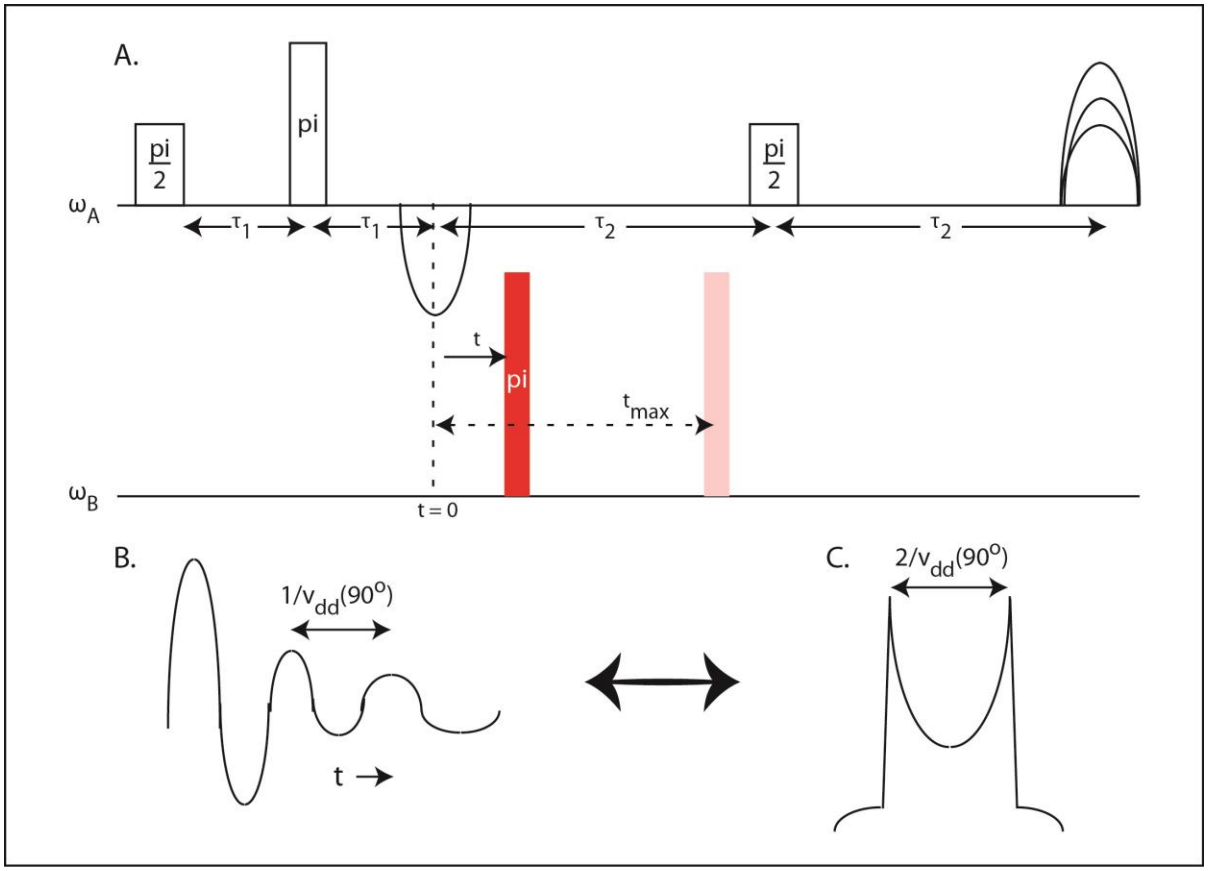

Figure 4: A) Pulse program for a 4-pulse DEER experiment. An initial π/2-pulse is applied at frequency ω_A and allowed to evolve for time τ_1 and then a π-pulse refocuses the spins producing a Han echo. A pump π-pulse at frequency ω_B at varying time, t, after the han echo modulates the observed spins. A final π-pulse at frequency ω_A refocuses the observed spins producing an echo whose amplitude is measured at time τ_2. B) Background corrected DEER experimental output with t corresponding to the position of the pump pulse. The dipolar frequency, ν_{dd}, can be measured from the oscillation frequency. C) Pake pattern resulting from Fast Fourier

Transform of the background corrected DEER trace. Often in real experiments the echo amplitude rapidly decays with t thus making oscillations difficult to pull directly from the background corrected trace. The distance between the pake pattern peaks is proportional to ν_{dd}.

III. Methods

3.1 Protein Expression

Purified DNA of Tau 187, Figure 1, consisting of residues 255-441 was transformed into *E. coli* BL21 (DE3) and grown in 10 mL of LB broth (Fisher Scientific) at 37 ^{o}C with shaking. This culture was used to inoculate a fresh 1 L batch of LB and was incubated at 37 ^{o}C with shaking until it reached an optical density of 0.6-0.8 at A_{600}. Expression of Tau 187 was then induced by adding 1 mM final isopropyl b-D-thiogalactopyranoside (IPTG, Fisher Scientific) and incubated for 3 hours. The bacteria were harvested by centrifugation at 4,500 x *g* (Beckman J-10) for 20 min.

1 Pierce protease inhibitor tablet (Thermo Scientific) and PMSF (1 mM) was added to lysis buffer (Tris-HCl, pH=7.4, 100 mM NaCl, 0.5 mM DTT, 0.1 mM EDTA). Cell pellets were dissolved in this mixture and incubated with lysozyme (2 mg mL^{-1}), DNase (20 mg mL^{-1}), and $MgCl_2$ (10 mM) and set on ice for 30 min. After lysis cells were sonicated for 20 min using a bath sonicator (Laboratory Supplies Co.). Cell debris was removed by centrifugation at 10,000 rpm at 4 ^{o}C for 10 min. The lysate was supplemented with an addition of PMSF (1 mM) and heated to 65 ^{o}C for 12 min. The samples were cooled on ice for 20 min and then centrifuged as described above to remove the precipitant. The supernatent was loaded onto a Ni-NTA agarose column, incubating overnight at 4°C. The Ni-NTA column was then equilibrated in wash buffer A (20 mM sodium phosphate, pH=7.0, 500 mM NaCl, 10 mM imidazole, 100 mM EDTA). The column was washed with 20 mL of buffer A, 15 mL buffer B (20 mM sodium phosphate, pH=7.0, 1 M NaCl, 20 mM imidazole, 0.5 mM DTT, 100 mM

EDTA), and then 10 mL of buffer A again. Purified protein was then eluted off the column in fractions with buffer C (20 mM sodium phosphate, pH=7.0, 0.5 mM DTT, 100 mM NaCl) supplemented with varying amounts of imidazole increasing from 100 mM to 300 mM. Fractions were analyzed by SDS-Page and those containing pure tau were pooled together. The protein was reduced with 5 mM DTT and precipitated by adding equal volume of methanol and incubating at -20 ^{o}C overnight. The resulting precipitated protein was then collected by centrifugation at 5,000 rpm at 4 ^{o}C for 45 min.

3.2 Spin Labeling

Tau was dissolved in 6 M guanidine hydrochloride and labeled by adding a 10 fold molar excess of spin label (1-oxyl-2,2,5,5,-tetramethylpyrroline-3-methyl) methanethiosulfonate (MTSL, Toronto Research Chemicals) or the diamagnetic analog of MTSL (1-Acetoxy-2,2,5,5,-tetramethyl-d-3-pyrroline-3-methyl) methanethiosulfonate (dMTSL, Toronto Research Chemicals). The labeling process was allowed to occur overnight at 4^{o}C. Excess label was removed by a PD-10 desalting column (GE Healthcare) equilibrated with desired buffer. The protein was then concentrated by centrifugation with 3kDa Amicon Ultra-4 Centrifugal Filters (Merck). Protein was then stored at -20°C.

3.3 Tht Fluorescence

Tht fluorescence intensity was measured with a Tecan M220 Infinite Pro plate reader at the Biological Nanostructures Laboratory within the California NanoSystems Institute (University of California, Santa Barbara). A 40uL sample volume was added to a Corning 384 Flat Black low volume well plate and covered with black vinyl electrical tape to prevent evaporation. A Fluorescence Intensity scan was run with excitation wavelength 450nm and emission wavelength 484nm. The excitation bandwidth was 9nm and emission bandwidth

was 20nm with an integration time of 20us. Number of flashes was set to 25. Readings were taken from the bottom and sampling was on a 1 min interval over a 16 hr period. A 500us settling time delay was applied.

3.4 cw-EPR

Cw-EPR was acquired using a Bruker EMX X-Band spectrometer and dielectric (ER4123D) cavity. The microwave source applied ~6 mW of power at 9.8 GHz using 0.3G modulation amplitude and sweep width of 150 gauss. Samples of 3.5uL volume were transferred to a 0.6mm diameter quartz capillary and sealed with wax on both ends. A 2-D EPR spectrum was then acquired stepping through time. Tau 187 322C concentration was 100uM, aggregation was induced with 25uM 11 kDa Heparin (Sigma Aldrich) in Phosphate Final buffer (20mM Sodium Phosphate, 100mM Sodium Chloride, 100uM EDTA, pH 7.0).

3.5 Turbidity

Turbidity measurements were carried out using a 8 multi-cell cuvette with a 1cm path length. A UV 1800 Shimadzu UV Spectrophotometer was used to acquire data at a 350nm wavelength. Sample volume was 100uL.

3.6 DEER Spectroscopy

DEER spectroscopy was carried out on doubly labeled tau with 75uM MTSL labeled tau and 825uM analog dMTSL labeled tau. The 1:11 MTSL:analog dMTSL ratio is meant eliminate interference from inter-protein spin interactions. Measurements were carried out in deuterated Phosphate Final buffer with 30wt% sucrose. 40uL samples were transferred to quartz sample tubes and flash frozen in liquid nitrogen. DEER measurements were carried out at 85K using a Bruker ELEXSYS E580 X-band spectrometer and MS3 resonator. A dead-time free four-pulse DEER sequence was used setting the pump pulse to the center of

the nitroxide spectrum and applying the observe pulse at 65 MHz higher frequency The pulse durations of the $(p/2)_{obs}$, $(p)_{obs}$, and $(p)_{pump}$, were 16 ns, 32 ns and 12 ns respectively. The delay t_1 was set to 200 ns while t_2 would vary from 1 ms up to 2 ms depending on the sample. Distance distributions were analyzed using DEERanalysis2013.

3.7 TEM

Aggregated tau solutions were fixed in 1.6% Gluteraldehyde (Electron Microscopy Sciences) for 15min. A TEM grid, FORMVAR Carbon film on 300 mesh copper (Electron Microscopy Sciences), was floated on 10uL of the fixed sample for 1min and then blotted on filter paper. The grid was touched to 10uL of Deionized water, blotted, touched to 10uL of the stain solution, 2% Uranyl Acetate, blotted and then floated on 10uL of 2% Uranyl Acetate (Electron Microscopy Sciences) for 1 minute before blotting and then setting aside to dry for 24hours. Imaging was carried out at room temperature using a JEOL JEM-1230 TEM at the UCSB NRI-MCDB Microscopy facility.

IV. Results and Discussion

4.1 β-Sheet Content Appears Early in Aggregation Process

Tht fluorescence and turbidity measurements, Figure 5, provide time resolved methods of monitoring the appearance of β-sheet content, however, Tht does not inform on the type of aggregate species—i.e. early oligomer vs fibrils—and a minimalistic Tht sensitive structure is unknown. Additionally, Tht is incapable of quantitatively informing on the population of tau embedded into β-sheet structure. Turbidity is dependent on particle size and morphology but offers no details of the molecular structure. Thus we apply cw-EPR to singly labeled tau protein which provides quantitative measurements of the tau population packed in parallel β-sheets. This specific packing structure is denoted by the appearance of a characteristic single line component in the typical three line nitroxide EPR spectra, Figure 3A, which is caused by close inter-spin distances of ~8 Å.[31, 37, 38] The total population of spins involved in these close distance spin-exchange interactions can be quantified from EPR

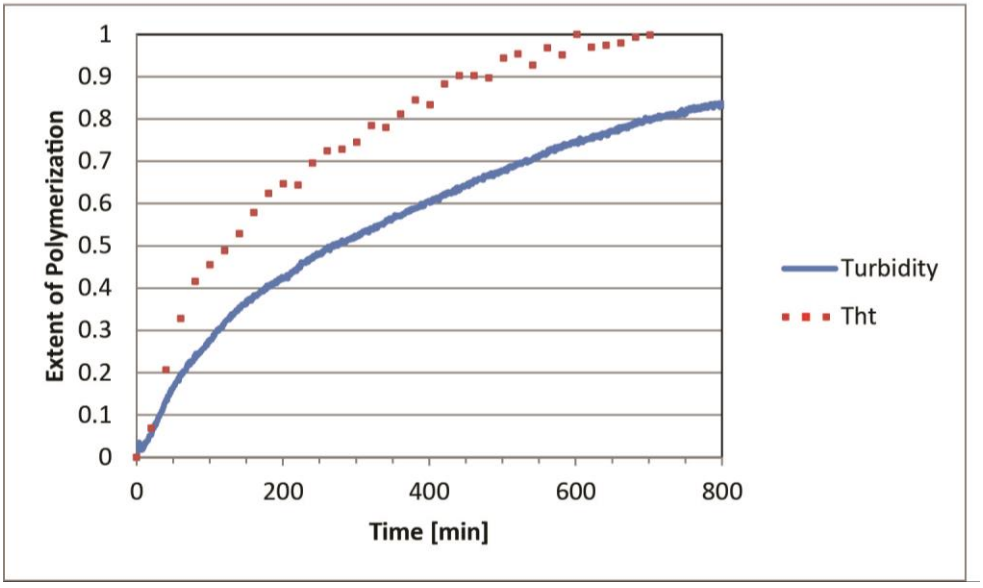

Figure 5: Comparison of kinetic curves derived by turbidity and Tht fluorescence. Sample conditions in both experiments 100uM Tau 187 322C, 25uM 11kDa heparin. In fluorescent experiment Tht concentration was 40uM. Fluorescence and turbidity measurement as described. Curves were normalized by maximum signal intensity and initial intensity was set to zero.

line shape decomposition of a 100% spin labeled tau sample, independent of fibril or oligomer size which is not necessarily true of Tht. Here we label Tau 187 with MTSL at the natural cysteine site 322 which has been previously demonstrated to exhibit spin-exchange upon aggregation into fibrils.[19, 39] Prior to heparin addition the Tau 187 322C MTSL EPR spectrum can be fit by a 100% mobile component, Figure 6. Line shape analysis of cw-EPR spectra immediately following heparin addition reveals spin-exchange interactions appear almost instantaneously. Within ~5min of aggregation induction ~10% of tau molecules are already embedded in parallel β-sheet structure as shown by the tau population involved in spin-exchange interactions (labeled β-sheet in Figure 6). The population of tau involved in spin-exchange interactions plateaus at ~65%, and an additional ~20% of tau has reduced spin label mobility. The amount of β-sheet structure plateaus after ~300min, Figure 6, but turbidity and Tht fluorescence, Figure 5, both continue to exhibit increases in signal intensity well after formation of new β-sheet structure has stagnated. This discrepancy further demonstrates turbidity and Tht fluorescence insensitivity to molecular scale structural changes and in the case of Tht fluorescence reiterates the uncertainty with regard to Tht binding principles.

The nature of early aggregate species is subject to debate as some studies indicate early oligomers are simply minimalistic aggregates with the same structure as mature fibrils, whereas more recent studies suggests early oligomers are a conformationally distinct species which later convert into fibrils through structural rearrangement.[16, 40-44] The cw-EPR data presented in Figure 6 unequivocally shows β-sheet structure forms during the earliest stages of aggregation well before fibrils are thought to exist. Despite the appearance of β-sheet structure early in the aggregation process, immediately after addition of heparin there is a

significant population of spins which have reduced mobility but are not directly involved in spin-exchange as shown by the large interfacial population, Figure 6. This could be indicative of rapid initial aggregation, resulting in reduced mobility of the spin label, which is followed by slower conversion to β-sheet structure as observed by the increase in spin-exchange interactions. This would be consistent with a model of aggregation which has nucleation followed by a structural rearrangement step. If early oligomers are indeed structurally distinct from fibrils, is there a detectable difference in behavior? The AD and tau community has become greatly interested in seeded aggregation, where pre-aggregates of tau are created and then added to naive tau. Considerable evidence has been compiled indicating the systematic propagation of tau pathology during AD as being carried out by pre-aggregates of tau.[21-28] Thus we specifically wish to examine the relationship between the population of tau embedded in β-sheet structure and seeding efficacy as well as determine whether the early aggregates in Figure 6 are on path-way.

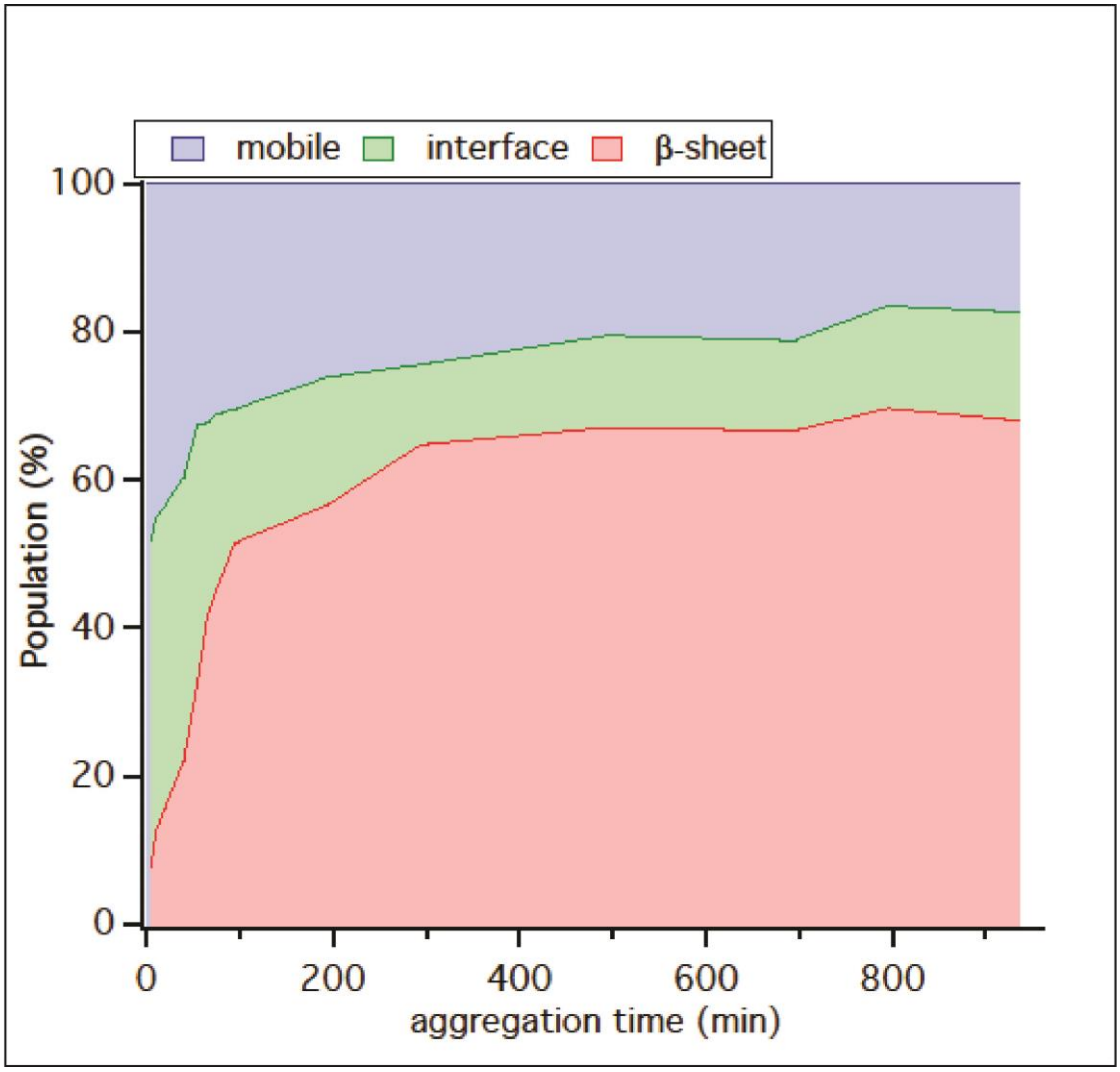

Figure 6: Population plot of Tau 187 322C 100% MTSL labeled during aggregation compiled from line shape analysis of cw-EPR spectra. β-sheet contribution refers to population of spins involved in spin-exchange interactions, while the interface component refers to broadening of the EPR line shape due to other effects. Note: 0 aggregation time is before heparin addition and is 100% mobile. Experimental conditions: 100uM Tau 187 322C MTSL, 25uM 11kDa Heparin Phosphate Final Buffer

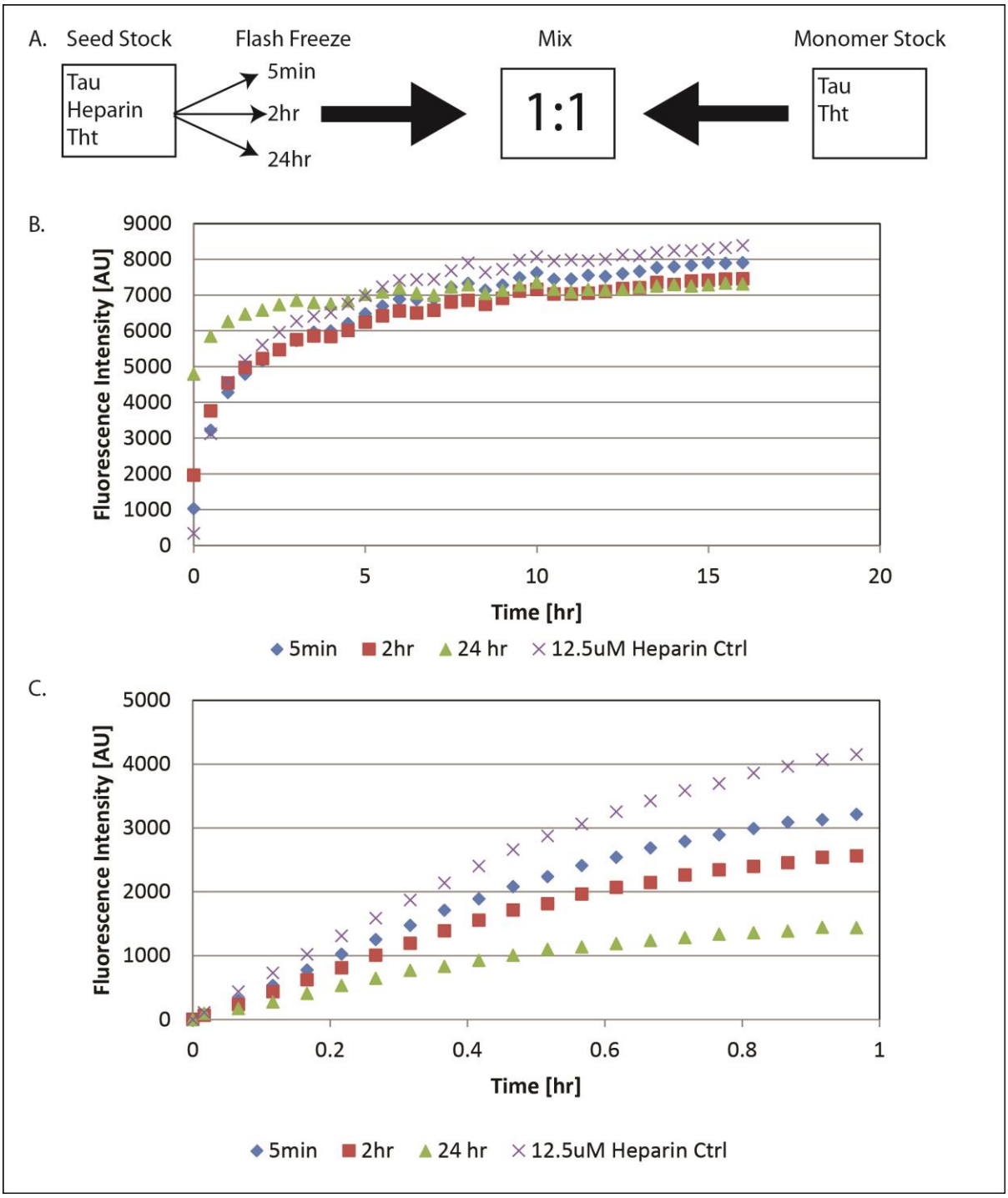

Figure 7: A) Schematic of seeding strategy. A seed stock was prepared with 100uM Tau 187 322C MTSL, 40uM Tht solution and incubated with 25uM 11kDa Heparin. Aliquots were removed at 5min, 2hrs, and 24hrs and flash frozen in liquid nitrogen. Aliquots were later thawed on ice and mixed in a 1:1 ratio with a monomer stock consisting of 100uM Tau 187 322C MTSL and 40uM Tht. The experiment was carried out in Phosphate Final Buffer. Fluorescence was then measured as described in methods. B)Tht Fluorescence of seed experiment with 5min, 2hr, and 24hr seeds mixed 1:1 with tau monomer as described. A control experiment consisting of the estimated residual heparin concentration was carried out mixing 100uM Tau 187 322C MTSL, 40uM Tht and 12.5uM Heparin in Phosphate Final Buffer.C) Same data as in B with emphasis on first hour of aggregation. Data was normalized by subtracting off initial fluorescence intensity of first data point in order to more clearly show difference in kinetic rate of aggregation between samples.

4.2 Pre-aggregated Species and Fibrils are not catalytic relative to heparin

The early appearance of β-sheet structure raises questions regarding the impact of early aggregate species on aggregation of naïve tau. Previous *in vitro* studies of seeded aggregation have focused on showing proof of concept, qualitative effects of seed concentration, and investigating conformational seeding barriers but none have addressed the fundamental question regarding the ability of different pre-aggregate species to recruit monomeric tau into fibrils.[16, 29, 30] In order to address this question we employ the general strategy outlined in Figure 7A, whereby a sample of tau is pre-aggregated with heparin, mixed in a 1:1 molar ratio with naive tau, and then monitored by Tht Fluorescence. Pre-aggregates with varying degrees of β-sheet content can be generated by modulating the incubation time with heparin. The 1:1 mixing of pre-aggregates with naïve tau should dilute the influence of heparin and through comparison to a control comprising the expected residual heparin concentration it should be possible to isolate the effect of pre-aggregated seed species.

The initial fluorescence intensity, Figure 7B, increases with incubation time of the pre-aggregated seeds, making apparent significant differences in the initial β-sheet content of the seed species. The cw-EPR data, Figure 6, shows ~10% of tau embedded in β-sheet structure at 5min, ~50% at 2hrs and ~65% at 24hrs. If Tht binding is linear with regard to parallel β-sheet structure the initial fluorescence intensity of the 2hr seeds should be approximately five times that of the 5min seeds and 24hr seeds should yield seven times the initial fluorescence of 5min seeds. It is clear such a straightforward correlation does not hold as 2hr seeds show roughly double the initial fluorescence intensity and 24hr seeds yield five times the initial intensity of the 5min seed sample. Therefore, we can conclude that Tht

fluorescence is non-linear with regard to parallel β-sheet content as quantified by cw-EPR. As aggregation proceeds a convergence to similar fluorescence intensity levels is observed across all samples, suggesting the extent of β-sheet content reaches a common amount independent of the initial seed species. This shows that Tht represents a quantifiable parameter, even if the exact nature of the species Tht intensity is measuring is unclear. Furthermore, these results confirm no additional irreversible off-pathway aggregates are created by the seeding process.

At first glance, seeds appear to retard the aggregation kinetics as shown by comparison of the initial kinetic rates, best illustrated in Figure 7C where the curves have been normalized by initial fluorescence intensity in order to more easily visualize differences in the slope. The unseeded sample shows the most rapid aggregation rate followed in order of increasing pre-aggregation time for the seed species. This is an observation inconsistent with past studies which have demonstrated pre-aggregated seeds are able to increase aggregation kinetics and reduce lag phases.[16] However, several key differences in experimental design hint at a possible explanation for this discrepancy. In the study by Friedhoff, P et al. the total tau concentration was not kept constant and the addition of seeds increased the total tau concentration relative to the unseeded control, thus there is more tau available to aggregate in their seeded vs unseeded experiments.[16] In our experimental design total tau concentration is held constant across all experiments. We suspect the differences in kinetic rate is not due to the seeds but rather to differences in the amount of tau available to aggregate, e.g. if we assume 24hr seeds are 65% aggregated initially (from Figure 6) and the heparin control is initially 0% aggregated (Figure 6) then the 24hr seed experiment would have 73.5% of tau available to aggregate and the heparin control would have 100% of tau

available to aggregate. A compounding factor which makes this difficult to directly assess from Tht Fluorescence is the non-linearity of fluorescence with respect to β-sheet structure as demonstrated by comparison of initial seed fluorescence intensity with cw-EPR. Therefore to draw a definitive conclusion would require conducting similar seeding experiments with cw-EPR as this would provide a direct measure of tau populations. Kinetic rates could then be measured based on the appearance of specific structural features rather than depend on a qualitative fluorescent marker. If differences in kinetic rate are indeed tied to available tau in solution, then it is heparin that ultimately is controlling the aggregation behavior and the effect of pre-aggregated seeds is being masked or overridden. Thus our next step is to examine the potency of heparin in promoting aggregation of tau.

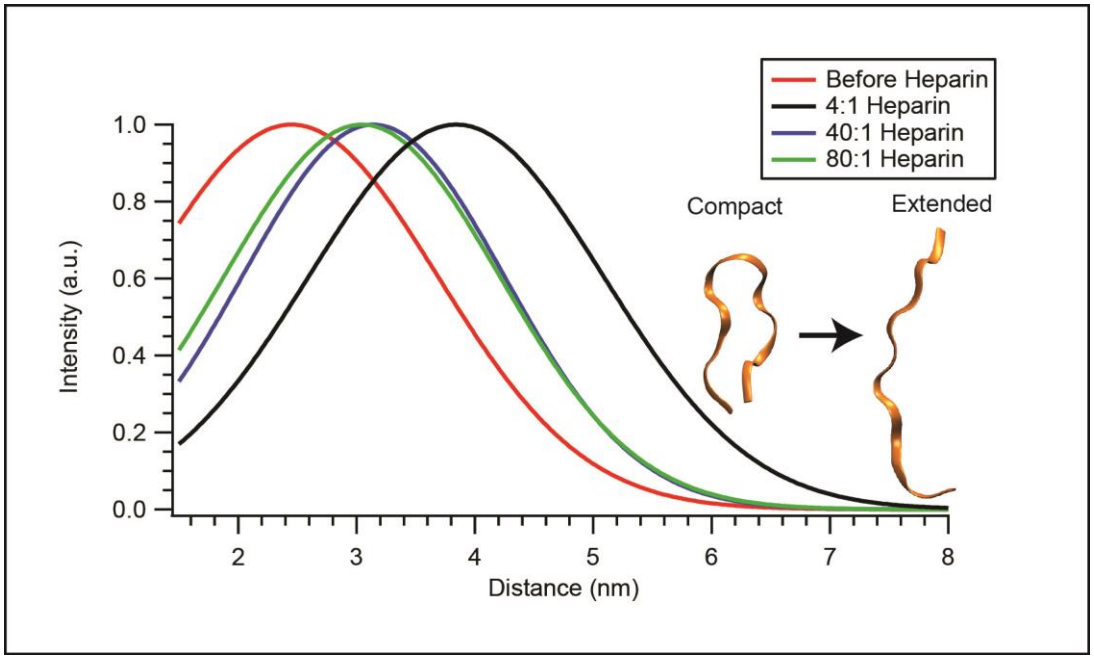

Figure 8: DEER distance distribution. Center of distribution represents average distance between attached spin labels. Tau 187 G272C/S284C MTSL 75uM, Tau187 G272C/S284C analog dMTSL 825uM, 11kDa Heparin various molar ratios, 30wt% sucrose in Phosphate Final Buffer in D_2O. Sampels aggregated for 1 hour and then flash frozen in liquid nitrogen. Measurement was carried out at 85 K. Inset schematic of extension from compact to extended state

4.3 Minute Amounts of Heparin are Capable of Extending Tau

The ability of heparin to override or mask the effect of pre-aggregated species as demonstrated in Figure 7 leads us to question the potency of heparin as a promoter of tau aggregation. Our group has identified a conformational shift around the PHF6* hexapeptide from a compact to an extended state, Figure 8 schematic, induced by mixing with heparin. In this work we specifically wish to address the nature of the tau-heparin interaction by examining the effect of stoichiometry on the aggregation process, hypothesizing that if heparin is acting in a catalytic like capacity then there should be no stoichiometric effect of heparin on the extension around PHF6* at least down to an unknown catalytic threshold. DEER spectroscopy contradicts this hypothesis as extension exhibits a stoichiometric dependence on heparin. A 4:1 tau:heparin ratio induces a more dramatic observable distance change compared to 40:1 or 80:1 ratio, Figure 8. Extension around the PHF6* hexapeptide is still observed at more dilute conditions, although the effect is reduced. Whether this reduction in extension distance is due to a smaller population being affected or resultant from a similar population undergoing a smaller conformational shift cannot be determined from DEER spectroscopy. A similar distance change is observed in both the 40:1 and 80:1 case so it does not appear that the stoichiometric dependence is linear. Commonly, a 4:1 molar ratio of tau:heparin is considered optimal for tau aggregation but our results show heparin is capable of inducing conformational rearrangement even at dilute conditions.[14] To further examine the stoichiometric effect of heparin we employ Tht to qualitatively examine the effect on tau aggregation kinetics.

4.4 Heparin Stoichiometry Dictates Total Amount of Fibril Content

Evidence from Figure 8 suggests a stoichiometric dependence between heparin and tau conformation around the PHF6* hexapeptide, but how does this dependence manifests in

the aggregation kinetics? Tht fluorescence exhibits a dependence on heparin stoichiometry, Figure 9, as higher heparin concentrations result in increased fluorescence and thus indicate increased fibril content, although cw-EPR would be required to quantify the exact differences in β-sheet amount. The dependence of observed distance change on heparin stoichiometry shown in Figure 8 has two possible explanations: 1) A smaller population of tau is extending, but the extension distance does not depend on heparin stoichiometry. 2) A similar tau population is affected but a lower heparin stoichiometry reduces how much tau extends. The results from Figure 9 seem to support the former explanation as a smaller amount of tau is involved in Tht active fibril formations at lower heparin concentrations. The fact that the amount of extension, Figure 8, correlates to the amount of fibril content, Figure 9, offers additional, though not conclusive, support to our hypothesis that the extension around the PHF6* hexapeptide is a critical step in the aggregation process.

The dependence of fibril content on heparin stoichiometry, Figure 9, corroborates a study by Ramachandran, G., and Udgaonkar, J. B.[45] They contribute this effect to a

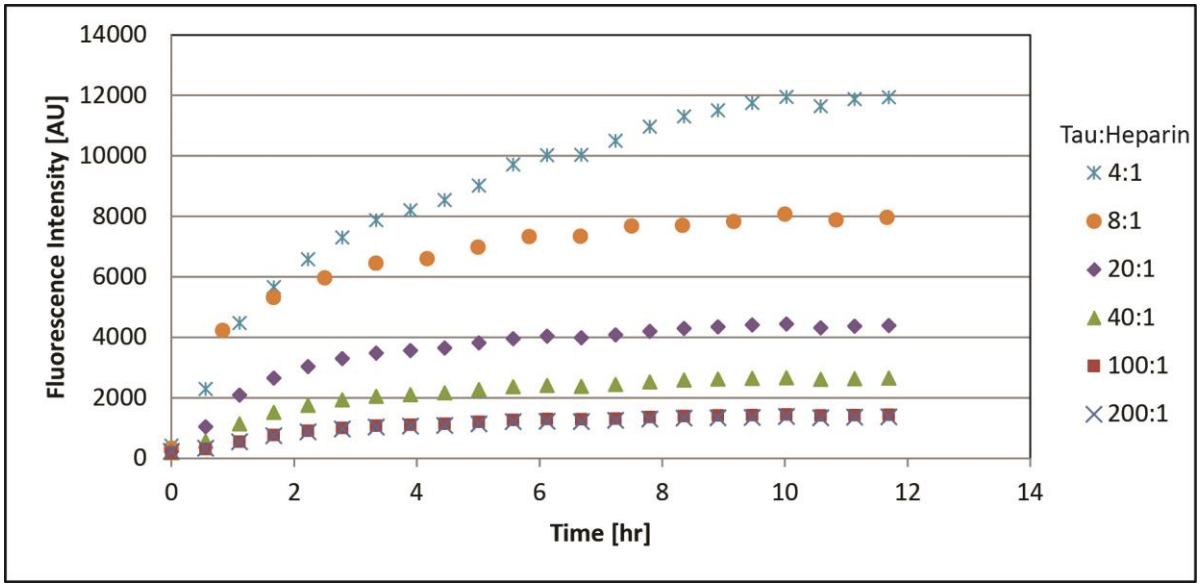

Figure 9: Tht Fluorescence of tau aggregation carried out at various tau:heparin stoichiometries. 100uM Tau 187 322C MTSL, 40uM Tht in Phosphate Final Buffer mixed with various concentrations of 11kDa Heparin. Tht fluorescence carried out as described.

stoichiometric complexation between tau and heparin in a 2:1 stoichiometric ratio. However, our observation of 40:1 and 80:1 tau:heparin ratios exhibiting similar distance changes, Figure 8, suggests a non-linear dependence of conformational rearrangement on stoichiometry thus an argument based on a defined tau:heparin complexation ratio seems too simplistic. Cw-EPR could provide some clarity in this regard by determining the precise dependence of parallel β-sheet structure on heparin stoichiometry, whereas Tht fluorescence is only capable of highlighting qualitative differences. Total fibril content and tau conformation both depend on heparin stoichiometry, but this dependence does not appear explainable by simple correlations and the tau-heparin relationship remains quite complex.

V. Conclusions

In this work we have examined the appearance of parallel β-sheet structure through a combination of Tht fluorescence, turbidity and cw-EPR. Our work demonstrates the drawbacks of Tht fluorescence and turbidity in sensitivity to molecular level details compared to cw-EPR which is capable of monitoring specific structural details of the aggregation system. As shown by our data in Figure 6 a small amount of β-sheet content appears immediately after heparin addition in conjuncture with a spike in the population of spins suffering decreased mobility. The following increase in spin-exchange interactions during aggregation is consistent with proposed models of aggregation which have initial nucleation followed by a structural rearrangement step. Subsequent seeding experiments corroborated early appearance of β-sheet structure but also showed Tht fluorescence to be non-linear with respect to β-sheet content measured by cw-EPR. Additionally, seeds do not affect end stage total fibril content. Differences in aggregation kinetics appear to be

dependent on the amount of tau available for aggregation and any effects of seeds on kinetic rate appear to be overridden by heparin.

The application of DEER spectroscopy revealed a stoichiometric dependence of tau conformational rearrangement around the PHF6* hexapeptide on heparin, however, even dilute heparin concentrations proved capable of inducing significant distance changes although the effect was reduced. The distance change dependence on stoichiometry appears to be non-linear as indicated by similar distance changes being observed at separate stoichiometries (40:1 and 80:1). Additionally, Tht fluorescence indicates a firm dependence between the total amount of fibril content and heparin stoichiometry. To quantitatively determine the exact dependence between β-sheet structure and heparin stoichiometry would require further investigation by cw-EPR. From our study it appears the nature of the tau-heparin aggregation system is quite complex and significant additional effort will be required to reach a full understanding.

VI. Future Work

Establishing the relationship between pre-aggregate seed structure and efficacy at recruiting naïve tau to aggregate is still an outstanding question of great importance to the field. Our work here has established the potency of heparin in controlling the aggregation of tau *in vitro* as heparin stoichiometry controls tau conformation rearrangement even at dilute quantities. Therefore it is necessary to find a method of removing heparin from pre-formed seeds or alternatively find a suitable method of creating seeds without using an induction cofactor. It has been reported that a disease mutant of tau, ΔK280, can be aggregated at experimentally relevant time scales through application of heat, thus aggregates formed from this ΔK280 mutant would be a good candidate for isolating the effect of seeds on kinetics.[46]

Finally, our work here has demonstrated the utility of cw-EPR to track aggregation kinetics as it provides molecular level resolution about the spin label environment. In future studies we should take advantage of these capabilities where quantitative population measurements are desirable.

VII. Acknowledgements

Z.R.O. would like to thank Professor Songi Han for her mentorship and providing direction to this project. Z.R.O. acknowledges support through the NIH Director's New Innovator award (1DP2OD007221-01) and support thanks to the generous gift of Paul and Cathie Slavik. The author made use of the NRI-MCDB Microscopy Facility and the Materials Research Laboratory Central Facilities supported by the NSF through the Materials Research Science and Engineering Centers (# DMR 1121053). The author acknowledges the use of the Biological Nanostructures Laboratory within the California NanoSystems Institute, supported by the University of California, Santa Barbara and the University of California, Office of the President. The MRL is a member of the NSF-funded Materials Research Facilities Network (www.mrfn.org). Figure 3 is a reproduction from a paper by Pavlova, A., et al.[47] Z.R.O. would like to thank Neil Eschmann for assistance with DEER spectroscopy experiments and productive discussion. Z.R.O would also like to thank Dr. Chi-Yuan Cheng for lending his expertise to this project and his assistance with analyzing cw-EPR line shape.

VIII. References

1. Association, A. s., 2014 Alzheimer's disease facts and figures. *Alzheimer's & Dementia* **2014,** 10, (2), e47-e92.
2. Götz, J.; Ittner, A.; Ittner, L. M., Tau-targeted treatment strategies in Alzheimer's disease. *British journal of pharmacology* **2012,** 165, (5), 1246-1259.
3. Golde, T. E.; Schneider, L. S.; Koo, E. H., Anti-aβ therapeutics in Alzheimer's disease: the need for a paradigm shift. *Neuron* **2011,** 69, (2), 203-213.
4. Hardy, J. A.; Higgins, G. A., Alzheimer's disease: the amyloid cascade hypothesis. *Science* **1992,** 256, (5054), 184.
5. Hardy, J.; Selkoe, D. J., The amyloid hypothesis of Alzheimer's disease: progress and problems on the road to therapeutics. *Science* **2002,** 297, (5580), 353-356.
6. Nisbet, R. M.; Polanco, J.-C.; Ittner, L. M.; Götz, J., Tau aggregation and its interplay with amyloid-β. *Acta neuropathologica* **2015,** 129, (2), 207-220.
7. Roberson, E. D.; Scearce-Levie, K.; Palop, J. J.; Yan, F.; Cheng, I. H.; Wu, T.; Gerstein, H.; Yu, G.-Q.; Mucke, L., Reducing endogenous tau ameliorates amyloid ß-induced deficits in an Alzheimer's disease mouse model. *Science* **2007,** 316, (5825), 750-754.
8. Braak, H.; Braak, E., Neuropathological stageing of Alzheimer-related changes. *Acta neuropathologica* **1991,** 82, (4), 239-259.
9. Mandelkow, E.-M.; Mandelkow, E., Biochemistry and cell biology of tau protein in neurofibrillary degeneration. *Cold Spring Harbor perspectives in medicine* **2012,** 2, (7), a006247.
10. Von Bergen, M.; Friedhoff, P.; Biernat, J.; Heberle, J.; Mandelkow, E.-M.; Mandelkow, E., Assembly of τ protein into Alzheimer paired helical filaments depends on a local sequence motif (306VQIVYK311) forming β structure. *Proceedings of the National Academy of Sciences* **2000,** 97, (10), 5129-5134.
11. Von Bergen, M.; Barghorn, S.; Biernat, J.; Mandelkow, E.-M.; Mandelkow, E., Tau aggregation is driven by a transition from random coil to beta sheet structure. *Biochimica et Biophysica Acta (BBA)-Molecular Basis of Disease* **2005,** 1739, (2), 158-166.
12. Garcia, M. L.; Cleveland, D. W., Going new places using an old MAP: tau, microtubules and human neurodegenerative disease. *Current opinion in cell biology* **2001,** 13, (1), 41-48.
13. Jeganathan, S.; von Bergen, M.; Mandelkow, E.-M.; Mandelkow, E., The Natively Unfolded Character of Tau and Its Aggregation to Alzheimer-like Paired Helical Filaments†. *Biochemistry* **2008,** 47, (40), 10526-10539.
14. Goedert, M.; Jakes, R.; Spillantini, M.; Hasegawa, M.; Smith, M.; Crowther, R., Assembly of microtubule-associated protein tau into Alzheimer-like filaments induced by sulphated glycosaminoglycans. *Nature* **1996**.
15. Hasegawa, M.; Crowther, R. A.; Jakes, R.; Goedert, M., Alzheimer-like changes in microtubule-associated protein Tau induced by sulfated glycosaminoglycans Inhibition of microtubule binding, stimulation of phosphorylation, and filament assembly depend on the degree of sulfation. *Journal of biological chemistry* **1997,** 272, (52), 33118-33124.
16. Friedhoff, P.; Von Bergen, M.; Mandelkow, E.-M.; Davies, P.; Mandelkow, E., A nucleated assembly mechanism of Alzheimer paired helical filaments. *Proceedings of the National Academy of Sciences* **1998,** 95, (26), 15712-15717.
17. Nilsson, M. R., Techniques to study amyloid fibril formation in vitro. *Methods* **2004,** 34, (1), 151-160.
18. Biancalana, M.; Koide, S., Molecular mechanism of Thioflavin-T binding to amyloid fibrils. *Biochimica et Biophysica Acta (BBA)-Proteins and Proteomics* **2010,** 1804, (7), 1405-1412.

19. Margittai, M.; Langen, R., Template-assisted filament growth by parallel stacking of tau. *Proceedings of the National Academy of Sciences of the United States of America* **2004,** 101, (28), 10278-10283.
20. Eschmann, N. A.; Do, T. D.; LaPointe, N. E.; Shea, J.-E.; Feinstein, S. C.; Bowers, M. T.; Han, S., Tau Aggregation Propensity Engrained in Its Solution State. *The Journal of Physical Chemistry B* **2015**.
21. Braak, H.; Del Tredici, K., The Pattern of Lesions During the Transition to the Symptomatic Phase and in Fully Developed Alzheimer's Disease. In *Neuroanatomy and Pathology of Sporadic Alzheimer's Disease*, Springer: 2015; pp 95-130.
22. Stancu, I.-C.; Vasconcelos, B.; Ris, L.; Wang, P.; Villers, A.; Peeraer, E.; Buist, A.; Terwel, D.; Baatsen, P.; Oyelami, T., Templated misfolding of Tau by prion-like seeding along neuronal connections impairs neuronal network function and associated behavioral outcomes in Tau transgenic mice. *Acta neuropathologica* **2015,** 129, (6), 875-894.
23. Michel, C. H.; Kumar, S.; Pinotsi, D.; Tunnacliffe, A.; St George-Hyslop, P.; Mandelkow, E.; Mandelkow, E. M.; Kaminski, C. F.; Kaminski Schierle, G. S., Extracellular monomeric tau protein is sufficient to initiate the spread of tau protein pathology. *J Biol Chem* **2014,** 289, (2), 956-67.
24. Frost, B.; Jacks, R. L.; Diamond, M. I., Propagation of tau misfolding from the outside to the inside of a cell. *Journal of biological chemistry* **2009,** 284, (19), 12845-12852.
25. Falcon, B.; Cavallini, A.; Angers, R.; Glover, S.; Murray, T. K.; Barnham, L.; Jackson, S.; O'Neill, M. J.; Isaacs, A. M.; Hutton, M. L., Conformation determines the seeding potencies of native and recombinant tau aggregates. *Journal of biological chemistry* **2015,** 290, (2), 1049-1065.
26. Dujardin, S.; Lécolle, K.; Caillierez, R.; Bégard, S.; Zommer, N.; Lachaud, C.; Carrier, S.; Dufour, N.; Aurégan, G.; Winderickx, J., Neuron-to-neuron wild-type Tau protein transfer through a trans-synaptic mechanism: relevance to sporadic tauopathies. *Acta Neuropathol Commun* **2014,** 2, (1), 14.
27. Iba, M.; Guo, J. L.; McBride, J. D.; Zhang, B.; Trojanowski, J. Q.; Lee, V. M.-Y., Synthetic tau fibrils mediate transmission of neurofibrillary tangles in a transgenic mouse model of Alzheimer's-like tauopathy. *The Journal of Neuroscience* **2013,** 33, (3), 1024-1037.
28. Mirbaha, H.; Holmes, B. B.; Sanders, D. W.; Bieschke, J.; Diamond, M. I., Tau trimers are the minimal propagation unit spontaneously internalized to seed intracellular aggregation. *Journal of biological chemistry* **2015**, jbc. M115. 652693.
29. Frost, B.; Ollesch, J.; Wille, H.; Diamond, M. I., Conformational diversity of wild-type Tau fibrils specified by templated conformation change. *Journal of biological chemistry* **2009,** 284, (6), 3546-3551.
30. Dinkel, P. D.; Siddiqua, A.; Huynh, H.; Shah, M.; Margittai, M., Variations in filament conformation dictate seeding barrier between three-and four-repeat tau. *Biochemistry* **2011,** 50, (20), 4330-4336.
31. Cobb, N. J.; Sönnichsen, F. D.; Mchaourab, H.; Surewicz, W. K., Molecular architecture of human prion protein amyloid: a parallel, in-register β-structure. *Proceedings of the National Academy of Sciences* **2007,** 104, (48), 18946-18951.
32. Jeschke, G., DEER distance measurements on proteins. *Annual review of physical chemistry* **2012,** 63, 419-446.
33. Fielding, A. J.; Heaven, G.; Hollas, M. A., New Developments in Spin Labels for Pulsed Dipolar EPR. *Molecules* **2014,** 19, (10), 16998-17025.
34. Pannier, M.; Veit, S.; Godt, A.; Jeschke, G.; Spiess, H. W., Dead-time free measurement of dipole–dipole interactions between electron spins. *Journal of Magnetic Resonance* **2011,** 213, (2), 316-325.
35. Jeschke, G.; Bender, A.; Paulsen, H.; Zimmermann, H.; Godt, A., Sensitivity enhancement in pulse EPR distance measurements. *Journal of Magnetic Resonance* **2004,** 169, (1), 1-12.

36. Jeschke, G.; Polyhach, Y., Distance measurements on spin-labelled biomacromolecules by pulsed electron paramagnetic resonance. *Physical Chemistry Chemical Physics* **2007,** 9, (16), 1895-1910.
37. Serag, A. A.; Altenbach, C.; Gingery, M.; Hubbell, W. L.; Yeates, T. O., Arrangement of subunits and ordering of β-strands in an amyloid sheet. *Nature Structural & Molecular Biology* **2002,** 9, (10), 734-739.
38. Jayasinghe, S. A.; Langen, R., Identifying structural features of fibrillar islet amyloid polypeptide using site-directed spin labeling. *Journal of biological chemistry* **2004,** 279, (46), 48420-48425.
39. Dinkel, P. D.; Holden, M. R.; Matin, N.; Margittai, M., RNA Binds to Tau Fibrils and Sustains Template-Assisted Growth. *Biochemistry* **2015**.
40. Shammas, S. L.; Garcia, G. A.; Kumar, S.; Kjaergaard, M.; Horrocks, M. H.; Shivji, N.; Mandelkow, E.; Knowles, T. P.; Mandelkow, E.; Klenerman, D., A mechanistic model of tau amyloid aggregation based on direct observation of oligomers. *Nat Commun* **2015,** 6.
41. Morris, A. M.; Watzky, M. A.; Finke, R. G., Protein aggregation kinetics, mechanism, and curve-fitting: a review of the literature. *Biochimica et Biophysica Acta (BBA)-Proteins and Proteomics* **2009,** 1794, (3), 375-397.
42. Morris, A. M.; Watzky, M. A.; Agar, J. N.; Finke, R. G., Fitting neurological protein aggregation kinetic data via a 2-step, minimal/“Ockham's razor” model: the Finke-Watzky mechanism of nucleation followed by autocatalytic surface growth. *Biochemistry* **2008,** 47, (8), 2413-2427.
43. Cremades, N.; Cohen, S. I.; Deas, E.; Abramov, A. Y.; Chen, A. Y.; Orte, A.; Sandal, M.; Clarke, R. W.; Dunne, P.; Aprile, F. A., Direct observation of the interconversion of normal and toxic forms of α-synuclein. *Cell* **2012,** 149, (5), 1048-1059.
44. Lee, J.; Culyba, E. K.; Powers, E. T.; Kelly, J. W., Amyloid-β forms fibrils by nucleated conformational conversion of oligomers. *Nature chemical biology* **2011,** 7, (9), 602-609.
45. Ramachandran, G.; Udgaonkar, J. B., Understanding the kinetic roles of the inducer heparin and of rod-like protofibrils during amyloid fibril formation by Tau protein. *Journal of biological chemistry* **2011,** 286, (45), 38948-38959.
46. Kumar, S.; Tepper, K.; Kaniyappan, S.; Biernat, J.; Wegmann, S.; Mandelkow, E.-M.; Müller, D.; Mandelkow, E., Stages and Conformations of Tau Repeat Domain during Aggregation and Effects on Neuronal Toxicity. *Journal of biological chemistry* **2014**, jbc. M114. 554725.
47. Pavlova, A.; Cheng, C.-Y.; Kinnebrew, M.; Lew, J.; Dahlquist, F. W.; Han, S., Protein structural and surface water rearrangement constitute major events in the earliest aggregation stages of tau. *Proceedings of the National Academy of Sciences* **2015**, 201504415.